Cellular and Molecular Life Sciences (2024) 81:436
https://doi.org/10.1007/s00018-024-05460-4

ORIGINAL ARTICLE

N6-methyladenosine-modified circCDK14 promotes ossification of the ligamentum flavum via epigenetic modulation by targeting AFF4

Yongzhao Zhao[1,2,3] · Longting Chen[1,2] · Qian Xiang[1,2,3] · Jialiang Lin[1,2,3] · Shuai Jiang[1,2,3] · Weishi Li[1,2,3]

Received: 30 October 2023 / Revised: 26 August 2024 / Accepted: 24 September 2024

Abstract

Background The ligamentum flavum (LF) is an important anatomical structure of the spine. Ossification of the LF (OLF) has become the leading cause of thoracic spinal stenosis. Circular RNAs (circRNAs) and N6-methyladenosine (m6A) modification are reported to be associated with several human diseases. However, the role of circRNAs and m6A modification in the pathogenesis of OLF has not been fully investigated. Here, we aimed to explore the vital function of circRNAs and m6A modification in OLF.

Materials and methods We analysed the circRNA expression of 4 OLF tissues and 4 normal LF tissues using bioinformatic analysis and identified circCDK14 for further analysis. We investigated the effects of circCDK14 on the osteogenic differentiation of LF cells. We observed that circCDK14 regulated its target genes by binding to miRNAs as a miRNA sponge. Moreover, the circRNA pull-down assay indicated that RNA-binding proteins might regulate the expression of circCDK14 via m6A modification.

Results CircCDK14 was significantly upregulated in OLF tissues compared to normal LF tissues. Overexpression of circCDK14 promoted the osteogenic differentiation of LF cells. Mechanistically, CircCDK14 promoted the expression of ALF transcription elongation Factor 4 (AFF4) by serving as a sponge for miR-93-5p. Moreover, Wilms tumour 1-associated protein (WTAP) increased the stability of circCDK14 via N6-methyladenosine modification.

Conclusion The m6A-modified CircCDK14 binding to miR-93-5p played an important role in the osteogenesis of LF cells by targeting AFF4, providing a promising therapeutic target for OLF.

Keywords Ossification of ligamentum flavum · CircCDK14 · MiRNAs sponges · N6-methyladenosine modification · Osteogenesis

Abbreviations

LF	Ligamentum flavum
OLF	Ossification of the ligamentum flavum
circRNAs	Circular RNAs
RBPs	RNA-binding proteins
WTAP	Wilms tumour 1-associated protein
IGF2BP3	Insulin-like growth Factor 2 mRNA-binding protein
AFF4	ALF transcription elongation Factor 4
PBS	Phosphate buffered saline
ALP	Alkaline phosphatase
ARS	Alizarin Red S
qRT-PCR	Quantitative real time polymerase chain reaction
MS2-CP	MS2-capturing protein
HEK	Human embryonic kidney
WT	Wild-type
MT	Mutant-type
siRNAs	Small interfering RNAs
SD	Standard deviation

Yongzhao Zhao, Longting Chen and Qian Xiang contributed equally to this research, and were listed as the co first authors.

✉ Weishi Li
puh3liweishi@bjmu.edu.cn

[1] Department of Orthopaedics, Peking University Third Hospital, Beijing, China

[2] Beijing Key Laboratory of Spinal Disease Research, Beijing, China

[3] Engineering Research Center of Bone and Joint Precision Medicine, Ministry of Education, 49 NorthGarden Road Haidian District, Beijing 100191, China

Published online: 16 October 2024

cDNA Complementary DNA
gDNA Genomic DNA

Introduction

The ossification of the ligamentum flavum (LF) (OLF), appearing in about 22% of the population, has become the leading cause of thoracic spinal stenosis [1]. The ossified ligamentum flavum can compress the spinal cord and lead to myelopathy, which manifests as sensation or motion abnormalities in the lower limbs [2]. It has been reported that several pathogenic factors may contribute to the onset or development of OLF, such as mechanical stress, ageing, obesity, and inflammation [3]. However, the underlying mechanisms of OLF are not fully understood to date.

Epigenetic modifications, which regulate gene expression without changing the DNA sequence, have been demonstrated to contribute to multiple human diseases, including musculoskeletal diseases [4, 5]. The epigenetic modifications mainly include noncoding RNAs, RNA modifications, DNA methylations, histone modifications, and chromatin remodelling [6]. Circular RNAs (circRNAs) are special noncoding RNAs characterized by their loop structure without 5′-3′ polarities and polyadenylated tails [7]. Circular RNAs are highly expressed in the nucleus and cytoplasm of eukaryotic cells and exert biological functions through the following forms: miRNA sponges, transcriptional regulation, interactions with RNA-binding proteins (RBPs), and translation into peptides [7]. The most common and important function of circRNAs is as miRNA sponges, where circRNAs regulate the level of targeted genes by sponging miRNAs [7, 8]. However, to the best of our knowledge, there is no research exploring whether circRNAs modulate the osteogenesis of LF cells by interacting with miRNAs to date. CircCDK14, also named hsa_circ_0001721, is derived from exon 3 of CDK14 and has a length of 246 bp. CircCDK14 has been demonstrated to play key roles in multiple diseases, such as glioma, osteosarcoma, and osteoarthritis [9–11].

N6-methyladenosine (m6A) modification is the most common RNA modification in higher eukaryotes and has attracted great attention in recent years [12, 13]. The m6A modification mainly includes methyltransferases (“writers”), demethylases (“erasers”), and binding proteins (“readers”) [13]. The core components of the RNA methyltransferase complex include methyltransferase-like 3, methyltransferase-like 14, and Wilms tumour 1-associated protein (WTAP), which add the m6A modification to the RNA [13]. In contrast, demethylases, including fat mass and obesity-associated protein and AlkB homologue 5, can remove the m6A modification on RNAs [13]. Reader proteins, such as insulin-like growth Factor 2 mRNA-binding protein 3 (IGF2BP3), can recognize the m6A modification in RNA and regulate the biosynthesis, nuclear export, stability, and translation of RNA [13]. Recently, many studies have demonstrated that m6A modification plays a significant role in the biosynthesis, nuclear export, and stability of circRNAs [14, 15]. Nevertheless, the vital role of m6A modification in the progression of OLF has not been fully investigated, especially when interacting with circRNAs.

In this study, for the first time, we found that circCDK14 is significantly increased in OLF tissues compared to normal LF tissues using circRNA microarray analysis. Mechanistically, we report that circCDK14 can bind to miR-93-5p as a miRNA sponge to elevate the expression of ALF transcription elongation Factor 4 (AFF4) and further promote the osteogenesis of LF cells. Furthermore, we found that increased WTAP expression increases the expression of circCDK14 through the WTAP/IGF2BP3 pathway.

Materials and methods

Clinical specimen collection

The experimental protocol was approved by the Ethics Committee of Peking University Third Hospital, and informed consent was obtained from each included patient. Control normal LF tissues were collected from patients undergoing percutaneous endoscopic lumbar discectomy for lumbar disc herniation. OLF tissues were collected from patients who underwent posterior laminectomy for thoracic spinal stenosis caused by OLF. The clinical specimens were either fixed in 4% paraformaldehyde or immediately frozen in liquid nitrogen after the surgery. The details of included patients in this study were listed in Supplementary Table 1.

LF cell isolation and culture

LF cells were isolated from freshly obtained LF tissues from OLF patients. First, the LF tissues were cut into small pieces of approximately 0.5 mm^3 and washed twice with phosphate buffered saline (PBS). The clipped tissue pieces were then digested with 0.25% trypsin (Gibco, USA) followed by 250 U/mL type I collagenase (Solarbio, China). After centrifugation, the sediment was resuspended in Dulbecco’s modified Eagle’s medium (Procell, China) containing 10% foetal bovine serum (Gibco, USA) and 1% penicillin/streptomycin antibiotics (Procell, China), which was subsequently placed in 10 cm culturing dishes in a humidified atmosphere with 5% CO_2 at 37 °C. The second and third passages of LF cells were used for subsequent experiments. For osteogenic differentiation, LF cells were cultured in commercial osteogenic medium provided by Procell (China).

RNase R treatment and RNA stability assay

Total RNA was extracted using a SteadyPure Universal RNA Extraction Kit (Accurate Biology, China). A total of 2 μg of RNA was incubated with or without RNase R at 37 °C for 10 min, which was used for the qRT−PCR assay. RNA stability was measured using the actinomycin D assay. LF cells were treated with 1 μg/mL actinomycin D (MCE, USA) for 0, 8, and 16 h, and then RNA was extracted from LF cells to determine the abundance of circCDK14.

Subcellular fractionation

The Ambion PARIS Kit (Invitrogen, USA) was applied for subcellular fractionation according to the manufacturer's instructions. GAPDH and U6 were employed as the cytoplasmic control and nuclear control, respectively.

RNA isolation and quantitative real time polymerase chain reaction (qRT-PCR) assay

Total RNA was extracted from LF cells using a SteadyPure Universal RNA Extraction Kit (Accurate Biology, China) following the manufacturer's protocol. First-strand cDNA was synthesized from 1.2 μg of total RNA using the Evo M-MLV RT Kit with gDNA Clean for qPCR kit (Accurate Biology, China). Then, the qRT−PCR assay was performed using the SYBR Green Premix Pro Taq HS qPCR Kit (Accurate Biology, China) on the ABI QuantStudio 5.0 version (Thermo Fisher Scientific, USA). The relative transcription levels were standardized to GAPDH using the $2^{-\Delta\Delta Ct}$ method. The primer sequences are listed in Supplementary Table 2.

Western blot and immunohistochemistry

LF cells or tissues were lysed with RIPA buffer (Epizyme, China), and the concentration of proteins was measured using the BCA kit (Epizyme, China) according to the manufacturers' protocol. After being denatured with loading buffer (Epizyme, China) at 99 °C for 15 min, protein samples were separated on 10% SDS–PAGE gels (Epizyme, China) and then transferred to polyvinylidene fluoride membranes (Millipore, USA) using Bio-Rad devices (Bio-Rad, USA). Then, the membranes were blocked with 5% skim milk powder (Epizyme, China) for 1.5 h and incubated with primary antibodies for 2 h at room temperature. The PVDF membranes were washed with TBST (Epizyme, China) and incubated with HRP-conjugated secondary antibodies (Epizyme, China) for 1 h at room temperature. An ECL kit (Epizyme, China) was used to visualize the immune complexes, and the relative protein levels were qualified using the iBright CL1000 device (Thermo Fisher Scientific, USA). The details of the preliminary antibodies used in this study were as follows: OPN (ImmunoWay, USA), RUNX2 (Abcam, USA), AFF4 (Proteintech, USA), AGO2 (Cell Signaling Technology, USA), and WTAP (Abcam, USA). For immunohistochemical staining, the formalin-fixed, paraffin-embedded LF tissues adjacent OLF tissues and normal LF tissues were analysed as previously reported [16], with the following preliminary antibodies: AFF4 (Proteintech, USA) and WTAP (Abcam, USA).

CircCDK14 pull-down assay and mass spectrometry analysis

The MS2 bacteriophage coat protein (MS2-CP) circRNA pull-down assay was conducted by using the MS2 tagging technique, and the MS2 tagging technique is developed for the natural binding between the stem-loop structure of MS2 and MS2-CP [28, 29]. In this study, the RBPs associated with circCDK14 were explored by using a circRNA pulldown assay with the MS2-CP technique. In brief, two specified plasmids were constructed: one plasmid with circCDK14-MS2 labelled with GFP, and another plasmid with MS2-CP-Flag labelled with mCherry. The HEK293T cells were transfected with these two plasmids and precipitated circCDK14 by the pulling down using anti-Flag antibodies. Besides, the lysates derived from the cells without the MS2 tagging system were used as the controls. The cell lysates were incubated with Protein A/G beads overnight at 4 °C. Then, the circCDK14-MS2-bound proteins were eluted. The bound RNA was reverse transcribed and analysed by qRT-PCR, and the bound proteins were determined by label-free mass spectrometry (Thermo Scientific, USA) and Western blot.

RNA immunoprecipitation (RIP) assay and methylated RNA immunoprecipitation (MeRIP) assay

The RIP experiment was conducted with the PureBinding® RNA Immunoprecipitation Kit (Geneseed, China) with anti-AGO2 (Cell Signaling Technology, USA) and WTAP (Abcam, USA) following the manufacturer's instructions. IgG (Cell Signaling Technology, USA) was used as a negative control. The coprecipitated circCDK14 level was further evaluated by qRT–PCR assay.

To detect the level of m6A modification in the circCDK14, MeRIP was conducted using the Magna MeRIP™ m6A kit (17–10–499, Merck Millipore, USA) according to the manufacturer's instructions. The m6A level of circCDK14 was evaluated using the qRT-PCR assay.

Dual-luciferase reporter assay assays

Human embryonic kidney (HEK) 293T cells were used for luciferase activity analysis and were plated on 96-well plates and cultured to 60–70% confluence. For circCDK14 and miR-93-5p, the circCDK14 fragments containing the complementary binding sites for miR-34a-5p were wild-type (WT) pMIR-REPORT-circCDK14 or mutant-type (MT) luciferase reporter pMIR-REPORT-circCDK14 (OBIO, China). Then, the luciferase reporter vectors of circCDK14-wt and circCDK14-mut, miR-93-5p mimics, and NC mimics were transfected using Lipofectamine 3000 (Invitrogen, USA). For AFF4 and miR-93-5p, the 3'UTR of AFF4 containing putative binding sites for miR-93-5p was cloned and inserted into the wild-type pMIR-REPORT-AFF4-3'UTR or mutant luciferase reporter pMIR-REPORT-AFF4-3'UTR (GemmaPharma, China). Then, the luciferase reporter vectors of AFF4-wt and AFF4-mut, miR-93-5p mimics, and NC mimics were transfected into HEK 293T cells. Luciferase activity was examined with a Dual Luciferase Reporter Assay kit (Promega, Beijing) following the manufacturer's instructions 48 h after transfection.

Small interfering RNA and plasmid construction and cell transfection

All small interfering RNAs (siRNAs) were provided by OBiO Technology (Shanghai, China). The miR-93-5p mimics were provided by OBiO Technology. The details of these siRNAs or mimics are listed in Supplementary Table 2. For the overexpression of circCDK14 and WTAP, the cDNA of circCDK14 and WTAP were synthesized, cloned, and inserted into the overexpression vector pcDNA3.1 by OBIO Technology as follows: pcDNA3.1(+), pcDNA3.1(+)-S-hsa_circ_0001721, pcDNA3.1(+)-3xFLAG-P2A-EGFP, and pcDNA3.1(+)-WTAP-3xFLAG-P2A-EGFP. All siRNAs, mimics, and vectors were transfected into LF cells with lipo3000 reagent following the manufacturer's protocols when LF cells reached 70% confluence. The LF cells were used for further experiments after the transfection.

Alkaline phosphatase (ALP) staining and activity assay

LF cells were seeded into 12-well plates at a density of 2.0×10^4 cells/well. ALP staining of LF cells was conducted using the BCIP/NBT Kit (Beyotime, China). According to the instructions, the cells were washed 3 times with cold PBS and then fixed in 4% paraformaldehyde for 15 min. Then, the fixed LF cells were washed 2–3 times with PBS again and added to ALP solution. After incubation in the dark for 30 min at room temperature, a stereomicroscope was used to capture the ALP staining images. The ALP activity of LF cells was assessed using the ALP/AKP kit (Nanjing Jiancheng, China) according to the instructions, and the OD was detected with a multiscan spectrum at an absorbance of 520 nm with an equal amount of protein.

Alizarin red s (ARS) staining and quantitative assay

Calcium deposition was assessed by ARS staining and quantitative assays during osteogenic differentiation. LF cells were inoculated into 12-well plates at a density of 2.0×10^4 / well. In brief, LF cells were fixed in 4% paraformaldehyde for 15 min 3 times with cold PBS. After rinsing with PBS 2–3 times, the cells were exposed to 0.20% ARS (Procell, China) solution and incubated shielded from light at room temperature for approximately 30 min. When the mineralization-positive cells were stained red, the cells were washed twice with PBS again, and photographs were captured under a stereomicroscope. After photographing, 10% cetylpyridine (Aladdin, China) was added to each well, followed by incubation under light protection at room temperature for 30 min. Then, the samples were transferred to 96-well plates at 100 µl per well, and the OD was detected with a microplate analyser (Thermo Fisher Scientific, USA) at an absorbance of 562 nm.

Statistical analysis

All analyses were conducted using GraphPad Prism 9.0 (GraphPad Software, USA), and all data are presented as the mean ± standard deviation (SD) of at least three independent experiments. Two-tailed unpaired Student's t test and one-way ANOVA followed by the Tukey–Kramer test were used to evaluate the statistical significance of any differences. $p<0.05$ was considered statistically significant.

Results

CircCDK14 was identified as an OLF-associated circular RNA

We performed bioinformatic analysis based on the GSE106255 dataset, and we observed that a total of 605 circRNAs were differentially expressed between normal LF tissues and OLF tissues (Supplementary Table 3) (Fig. 1A). Among the significantly increased circRNAs, we paid special attention to circCDK14, also known as hsa_circ_0001721, which was reported to play key roles in several human diseases [11, 17]. However, whether circCDK14 is involved in LF osteogenesis has not been investigated. To validate the results of the bioinformatic analysis, qRT-PCR assay was conducted, and we confirmed that circCDK14 expression was significantly increased in OLF

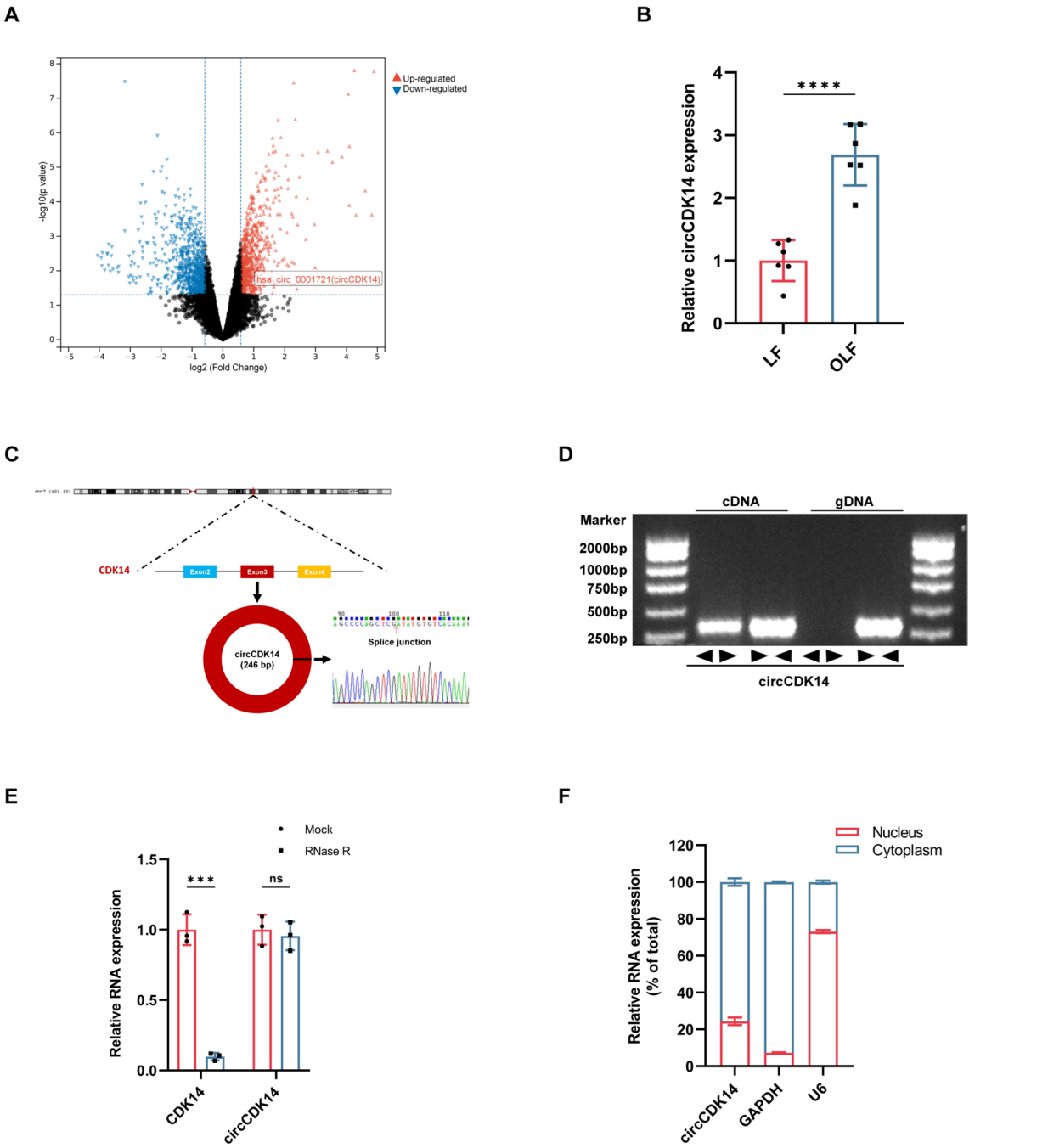

Figure 1 CircCDK14 was characterized as a OLF-related circular RNA. **A** The volcano plot of the differentially expressed circRNAs between OLF tissues and normal LF tissues. **B** CircCDK14 expression was significantly increased in OLF tissues compared to normal LF tissues. **C** CircCDK14 is looped by CDK14 exon 3, and verified by Sanger sequencing. **D** Products amplified using divergent (← →) or convergent (→←) primers of circCDK14. **E** Relative abundance of circCDK14 and CDK14 with or without RNase R treatment. **F** The nuclear and cytoplasmic fractions of circCDK14, GAPDH, and U6. *LF*, ligamentum flavum; *OLF*, ossification of the ligamentum flavum

tissues compared to normal LF tissues (Fig. 1B). According to the annotation information in the circBase database, circCDK14 was generated by the circularization of exon 3 of the CDK14 gene with a length of 246 bp and a position of chr7:90355880–90,356,126 (Fig. 1C). Gel electrophoresis of complementary DNA (cDNA) and genomic DNA (gDNA) from LF cells was performed, and the results revealed that circCDK14 could only be amplified by divergent primers in cDNA, and no product was observed in the gDNA groups (Fig. 1D). Besides, circCDK14 was resistant to digestion by RNase R, which further confirmed the ring structure of circCDK14 (Fig. 1E). In addition, qRT-PCR analysis of nuclear

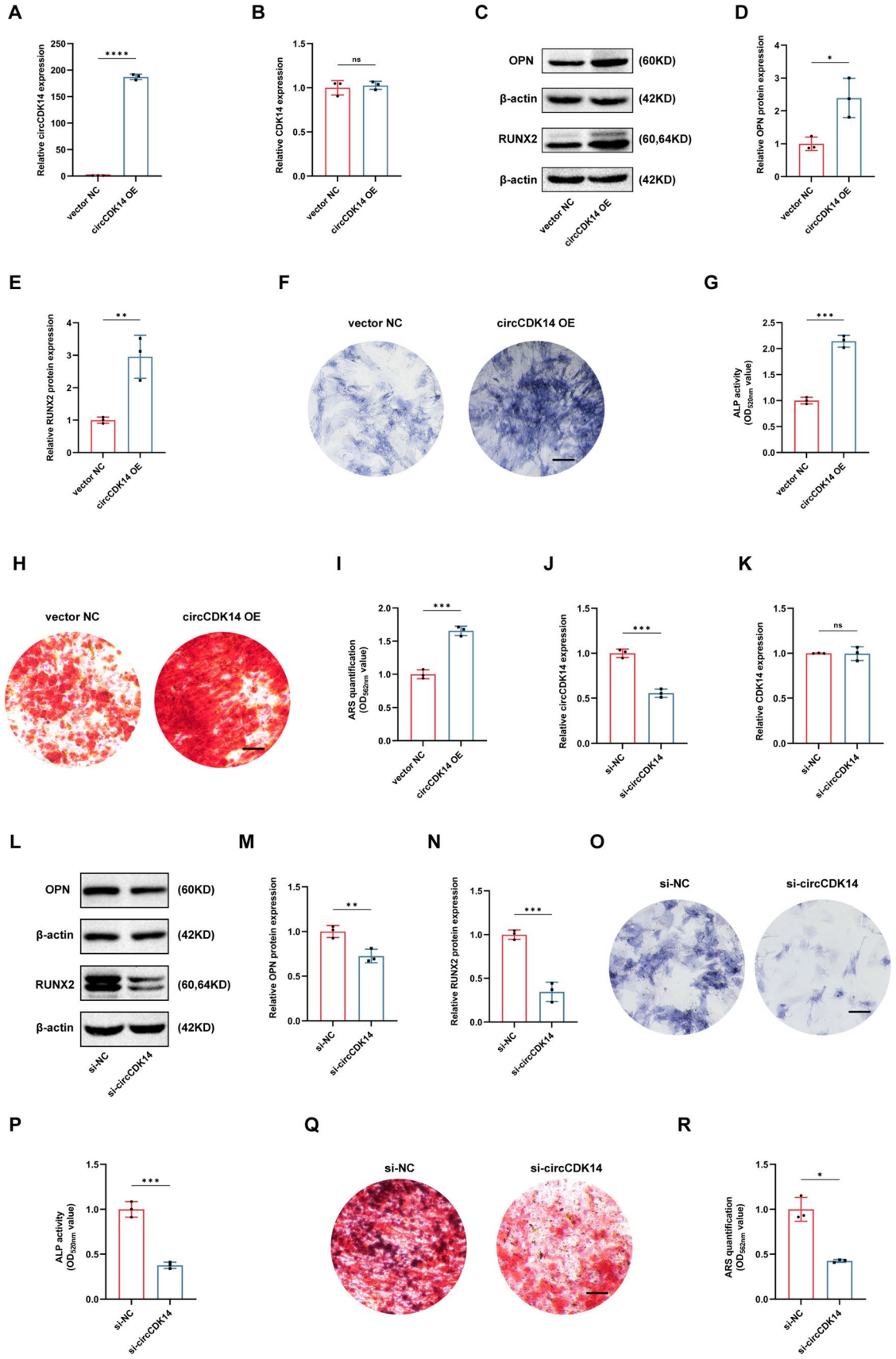
A
Relative circCDK14 expression
****
vector NC
circCDK14 OE
B
Relative CDK14 expression
ns
vector NC
circCDK14 OE
C
OPN
(60KD)
β-actin
(42KD)
RUNX2
(60,64KD)
β-actin
(42KD)
vector NC
circCDK14 OE
D
Relative OPN protein expression
*
vector NC
circCDK14 OE
E
Relative RUNX2 protein expression
**
vector NC
circCDK14 OE
F
vector NC
circCDK14 OE
G
ALP activity (OD520nm value)
***
vector NC
circCDK14 OE
H
vector NC
circCDK14 OE
I
ARS quantification (OD562nm value)
***
vector NC
circCDK14 OE
J
Relative circCDK14 expression
***
si-NC
si-circCDK14
K
Relative CDK14 expression
ns
si-NC
si-circCDK14
L
OPN
(60KD)
β-actin
(42KD)
RUNX2
(60,64KD)
β-actin
(42KD)
si-NC
si-circCDK14
M
Relative OPN protein expression
**
si-NC
si-circCDK14
N
Relative RUNX2 protein expression
***
si-NC
si-circCDK14
O
si-NC
si-circCDK14
P
ALP activity (OD520nm value)
***
si-NC
si-circCDK14
Q
si-NC
si-circCDK14
R
ARS quantification (OD562nm value)
*
si-NC
si-circCDK14

◂**Figure 2** CircCDK14 promoted the osteogenic differentiation of LF cells. **A**, **B** RNA level of circCDK14 and CDK14 after transfecting LF cells with circCDK14 overexpression vector. **C**, **E** Protein levels of osteogenic markers (OPN and RUNX2) after the circCDK14 overexpression. **F**–**I** ALP (**F**, **G**) and ARS (**H**, **I**) intensity after the circCDK14 overexpression (Scale bar = 25 μm). **J**, **K** RNA level of circCDK14 and CDK14 after the circCDK14 knockdown. **L**–**N** Protein levels of osteogenic markers (OPN and RUNX2) after the circCDK14 knockdown. **O**–**R** ALP (**O**, **P**) and ARS (**Q**, **R**) intensity after the circCDK14 knockdown (Scale bar = 25 μm). *OE*, overexpression; *ALP*, alkaline phosphatase; *ARS*, Alizarin Red S; * $p < 0.05$, ** $p < 0.01$, *** $p < 0.001$, *ns*, not significant

and cytoplasmic fractions showed that circCDK14 was predominantly located in the cytoplasm in LF cells (Fig. 1F).

CircCDK14 promoted the osteogenic differentiation of LF cells

To further explore the role of circCDK14 in the osteogenic differentiation of LF cells, we used an overexpression vector and siRNAs to overexpress and knock down circCDK14 in LF cells, respectively. We transfected LF cells with a circCDK14 overexpression vector, and qRT-PCR assays showed that circCDK14 expression was significantly increased without the alteration of CDK14 expression (Fig. 2A, B). Western blot analysis showed that circCDK14 overexpression significantly elevated the expression levels of osteogenic markers (OPN and RUNX2) (Fig. 2C–E). Moreover, LF cells treated with the circCDK14 overexpression vector exhibited greatly increased ALP (Fig. 2F and G) and ARS (Fig. 2H and I) intensity compared with the negative control, indicating an elevated osteogenic differentiation capacity. In contrast, when we transfected circCDK14 siRNA targeting the junction site of circCDK14 into LF cells, the qRT−PCR results showed that circCDK14 siRNA inhibited the expression of circCDK14 but had no obvious effect on the expression level of CDK14 (Fig. 2J and K). Western blot analysis showed that circCDK14 siRNA significantly reduced the protein levels of osteogenic markers (OPN and RUNX2) (Fig. 2L–N). Inhibition of circCDK14 in LF cells obviously reduced the ALP (Fig. 2O and P) and ARS (Fig. 2Q and R) intensity compared to that in the negative control. Taken together, our data suggested that circCDK14 could promote the osteogenic differentiation of LF cells.

CircCDK14 served as a sponge for mir-93-5p in LF cells

circCDK14 was mainly located in the cytoplasm; therefore, we speculated that circCDK14 might promote OLF by sponging miRNAs. According to the starBase database, miR-93-5p was a potential target of circCDK14 (Fig. 3A). The qRT-PCR assay results showed that miR-93-5p was obviously decreased in OLF tissues compared with normal LF tissues (Fig. 3B). To confirm the association between circCDK14 and miR-93-5p, we performed anti-AGO2 RIP in human LF cells and observed that circCDK14 pulled down by the anti-AGO2 antibody was significantly enriched compared to that pulled down by the control IgG antibody (Fig. 3C). Moreover, a circCDK14 fragment with wild-type or mutant complementary binding sites for miR-93-5p was constructed and inserted into luciferase reporter vectors. The results of the luciferase reporter assay showed that miR-93-5p overexpression significantly suppressed the luciferase activity of the WT reporter but not that of the MUT reporter, suggesting that circCDK14 was directly bound by miR-93-5p via the complementary target sites (Fig. 3D). Moreover, we transfected LF cells with circCDK14 overexpression vectors and siRNAs to increase and decrease the level of circCDK14 in LF cells, respectively. We discovered that circCDK14 overexpression significantly reduced the expression level of miR-93-5p compared to that in the control group. In contrast, the reduction in circCDK14 expression obviously elevated the miR-93-5p level (Fig. 3E and F). Therefore, our results showed that miR-93-5p is the downstream regulator of circCDK14 during osteogenesis in LF cells.

To determine the role of miR-93-5p in the osteogenesis of LF cells, we transfected LF cells with miR-93-5p mimics, and qRT−PCR analysis indicated that the level of miR-93-5p was significantly increased after the transfection of miR-93-5p mimics (Fig. 3G). The overexpression of miR-93-5p obviously decreased the expression of osteogenic markers (OPN and RUNX2) (Fig. 3H–J). Moreover, the overexpression of miR-93-5p reduced the ALP (Fig. 3K and L) and ARS (Fig. 3M and N) intensity compared to the negative control.

MiR-93-5p repressed AFF4 expression by targeting the 3′-UTR of AFF4

To explore the potential targets of miR-93-5p, we conducted the bioinformatic analysis based on the Starbase database. Among the potential targets of miR-93-5p predicted by Starbase database, we paid the special attention to the AFF4 for the reason that it has been reported to be associated with the osteogenesis (Fig. 4A) [18, 19]. To further explore the role of AFF4 in the pathogenesis of OLF, we conducted qRT-PCR and immunohistochemical analysis to determine the expression of AFF4 during the pathogenesis of OLF, and the results showed that the mRNA (Fig. 4B) and protein (Fig. 4C) levels of AFF4 were significantly increased in OLF tissues compared to normal LF tissues. To confirm the relationship between miR-93-5p and AFF4, we constructed a luciferase reporter vector with the WT or MUT AFF4 3'-UTR possessing the putative miR-93-5p target site. We discovered that

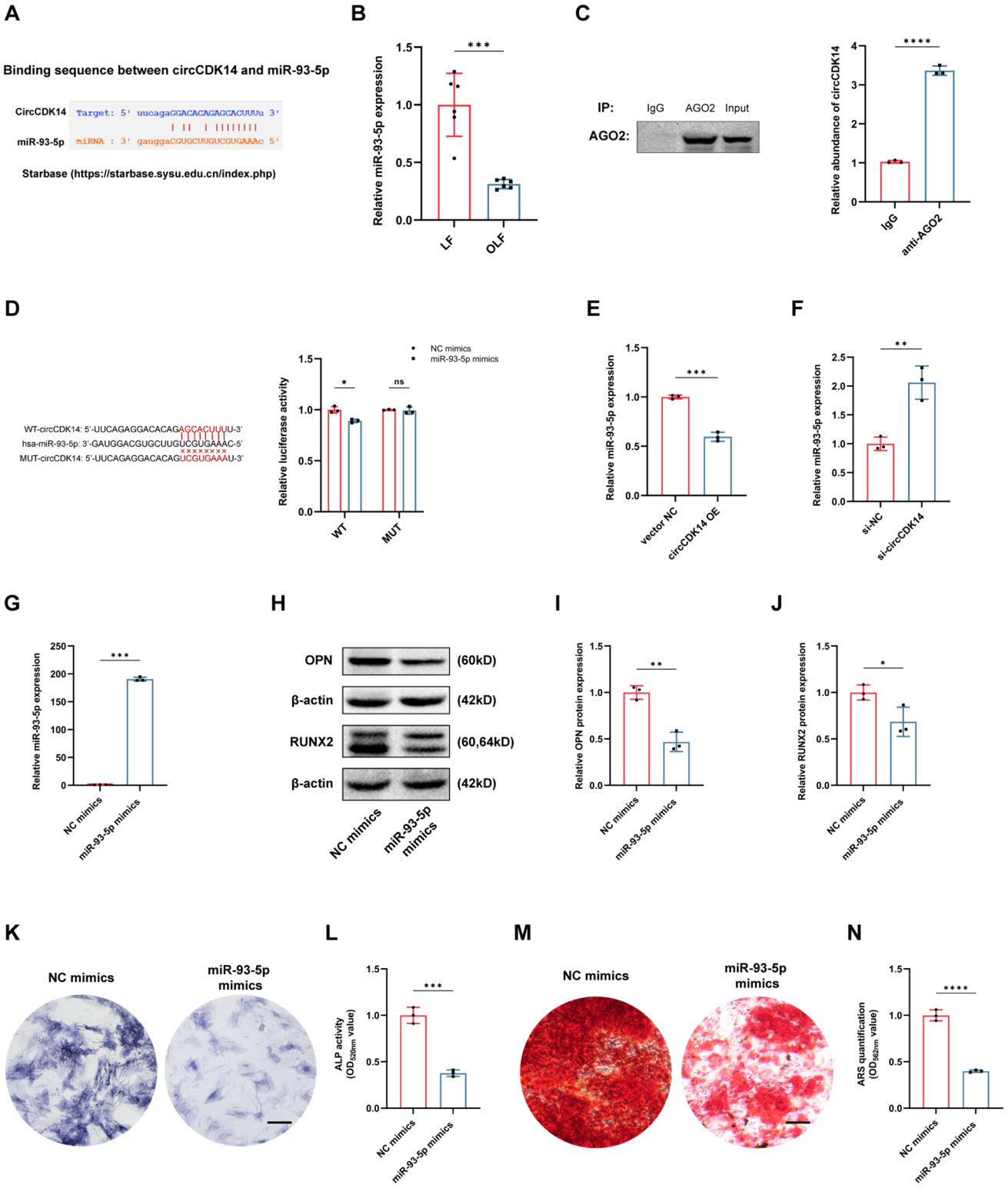

Figure 3 CircCDK14 served as a sponge for miR-93-5p in LF cells. **A** Bioinformatic analysis indicating miR-93-5p is a potential target of circCDK14. **B** RNA level of miR-93-5p in LF or OLF tissues. **C** CircCDK14 pulled down by the anti-AGO2 antibody. **D** Luciferase reporter activity of circCDK14 in HEK-293T cells co-transfected with miR-93-5p mimics or mimics control. **E**, **F** RNA level of miR-93-5p after the overexpressing (**E**) or silencing (**F**) the circCDK14. **G** RNA level of miR-93-5p after the transfection of miR-93-5p mimics. **H**–**J** Protein levels of osteogenic markers (OPN and RUNX2) after the transfection of miR-93-5p mimics. **K**–**N**) ALP (**K**, **L**) and ARS (**M**, **N**) intensity after the transfection of miR-93-5p mimics (Scale bar = 25 μm). *ALP*, alkaline phosphatase; *ARS*, Alizarin Red S; * $p < 0.05$, ** $p < 0.01$, *** $p < 0.001$, **** $p < 0.0001$, *ns*, not significant

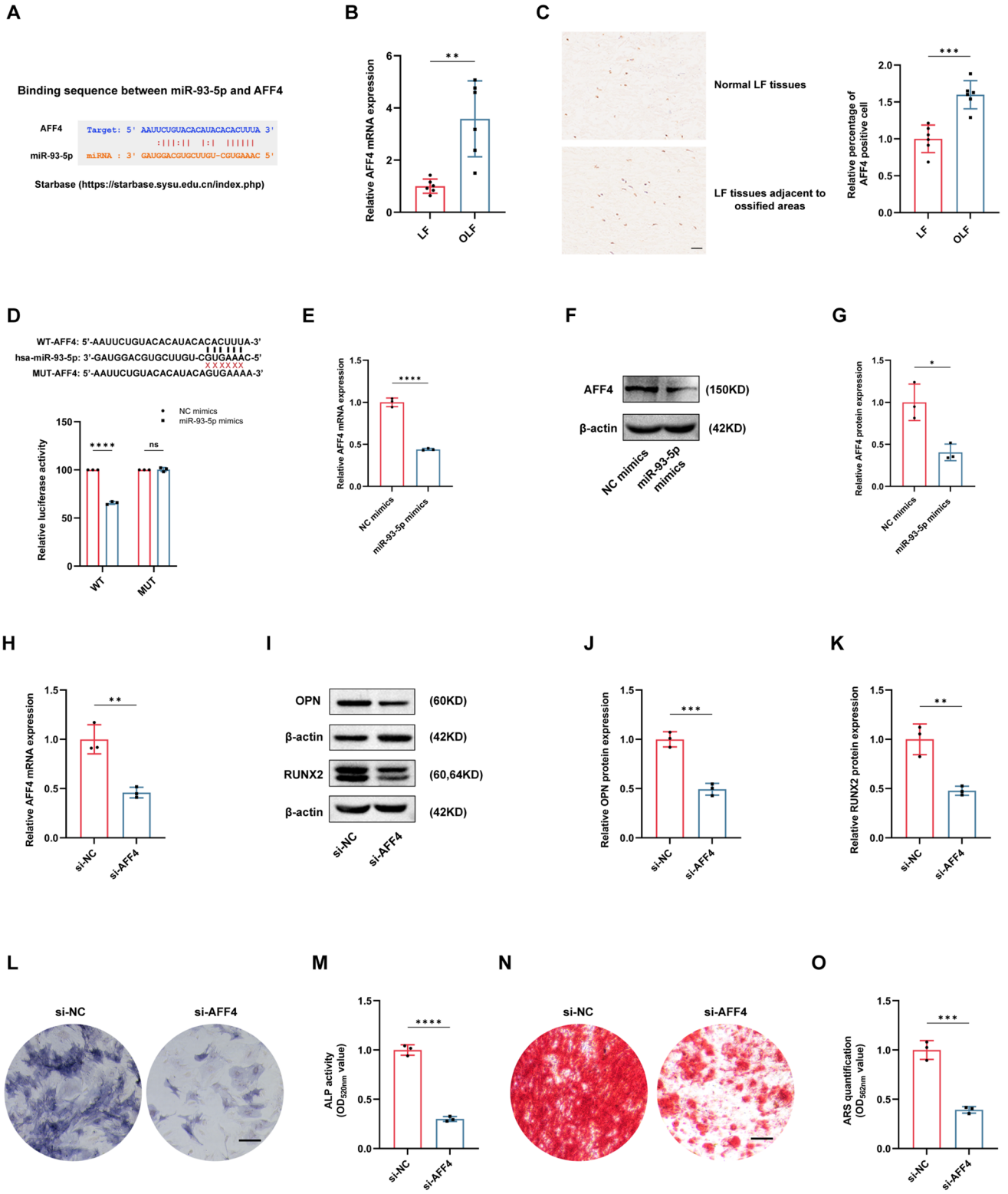

Figure 4 MiR-93-5p repressed the AFF4 expression by targeting the 3'-UTR of AFF4. **A** Bioinformatic analysis indicating that AFF4 is a potential target of miR-93-5p. **B**, **C** mRNA (**B**) and protein (**C**) levels of AFF4 in LF or OLF tissues (Scale bar = 50 μm). **D** Luciferase reporter activity between AFF4 and miR-93-5p. **E**, **G** mRNA (**E**) and protein levels (**F**, **G**) of AFF4 after the transfection of miR-93-5p mimics. **H** mRNA level of AFF4 after the transfection of siRNAs targeting AFF4. **I**–**K** Protein level of osteogenic markers (OPN and RUNX2) after the AFF4 knockdown. **L**–**O** ALP (**L**, **M**) and ARS (**N**, **O**) intensity after the AFF4 knockdown (Scale bar = 25 μm). *LF*, ligamentum flavum; *OLF*, ossification of the ligamentum flavum; *ALP*, alkaline phosphatase; *ARS*, Alizarin Red S; * $p < 0.05$, ** $p < 0.01$, *** $p < 0.001$, *ns*, not significant

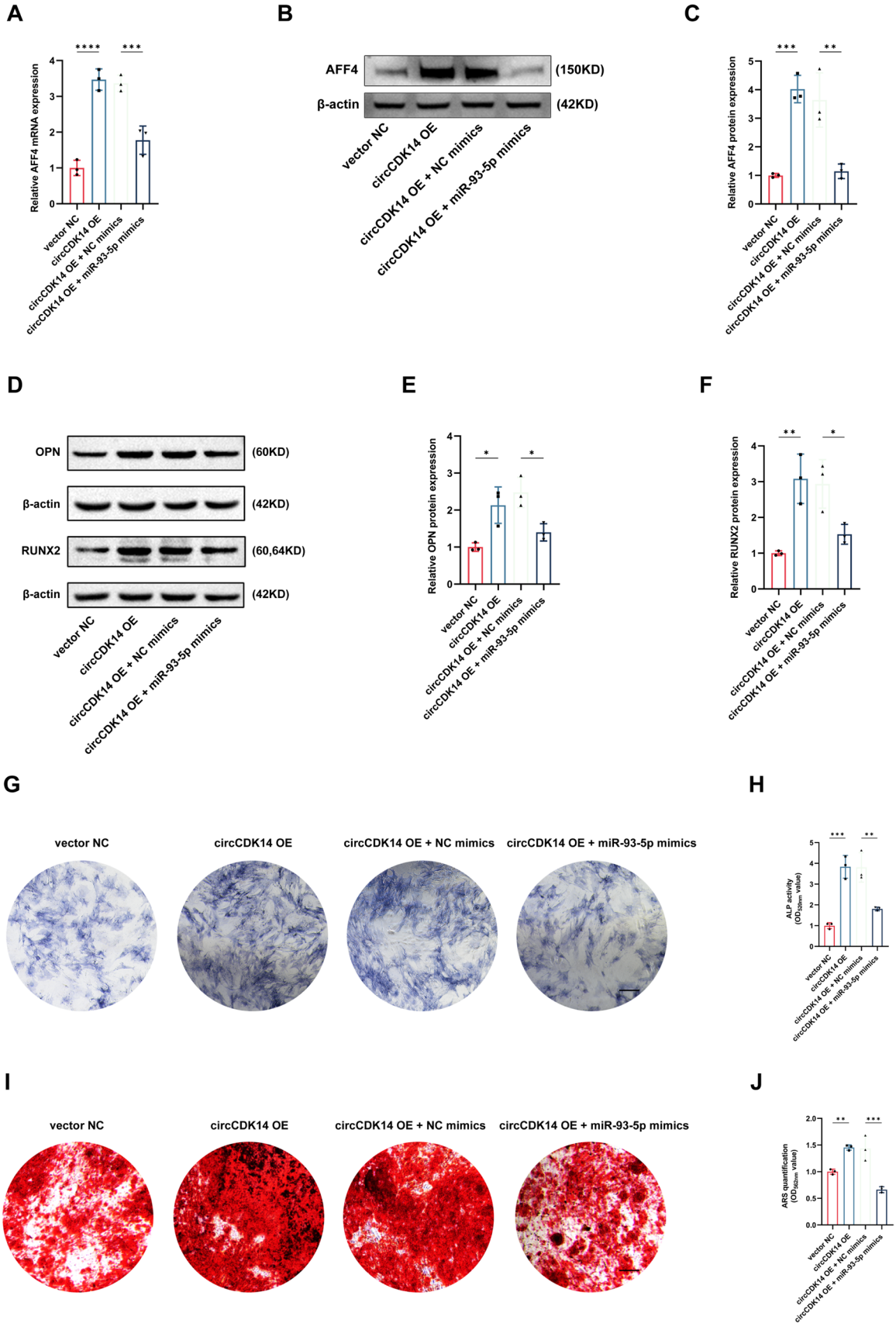
A
Relative AFF4 mRNA expression
vector NC
circCDK14 OE
circCDK14 OE + NC mimics
circCDK14 OE + miR-93-5p mimics
B
AFF4
(150KD)
β-actin
(42KD)
C
Relative AFF4 protein expression
D
OPN
(60KD)
β-actin
(42KD)
RUNX2
(60,64KD)
E
Relative OPN protein expression
F
Relative RUNX2 protein expression
G
H
ALP activity
I
J
ARS quantification

◂**Figure 5** CircCDK14 modulated the osteogenesis of LF cells via the miR-93-5p/AFF4 pathway (**A**–**C**) mRNA (**A**) and protein levels (**B**, **C**) of AFF4 after the co-transfection of circCDK14 overexpression vector and miR-93-5p mimics. (**D**–**F**) Protein levels of osteogenic markers (OPN and RUNX2) after the co-transfection of circCDK14 overexpression vector and miR-93-5p mimics (**G**–**J**) ALP (**G**, **H**) and ARS (**I**, **J**) intensity after the co-transfection of circCDK14 overexpression vector and miR-93-5p mimics (Scale bar = 25 μm). *OE*, overexpression; *ALP*, alkaline phosphatase; *ARS*, Alizarin Red S; * $p < 0.05$, ** $p < 0.01$, *** $p < 0.001$; **** $p < 0.0001$; *ns*, not significant

miR-93-5p overexpression could obviously decrease the luciferase activity of the reporter containing the WT 3'-UTR of AFF4 compared to the mimic control. However, no significant change in luciferase activity was detected in the MUT 3'-UTR of AFF4 group (Fig. 4D). Moreover, to further confirm the association between miR-93-5p and AFF4, we performed qRT−PCR and Western blot assays, and we observed that miR-34a-5p overexpression remarkably inhibited AFF4 mRNA (Fig. 4E) and protein (Fig. 4F and G) expression in LF cells. All data indicated that miR-93-5p could directly bind to the 3'-UTR of AFF4 and negatively regulate its expression. Then, we transfected LF cells with siRNA targeting AFF4, and qRT-PCR analysis confirmed the reduced expression of AFF4 after transfection (Fig. 4H). Western blot analysis showed that the reduction in AFF4 expression decreased the protein levels of osteogenic markers (OPN and RUNX2) in LF cells (Fig. 4I–K). In addition, the knockdown of AFF4 obviously reduced the ALP (Fig. 4L and M) and ARS (Fig. 4N and O) intensity compared to the negative control.

CircCDK14 modulated the osteogenesis of LF cells via the miR-93-5p/AFF4 pathway

To further confirm the combined effect of circCDK14 and miR-93-5p on AFF4, we used qRT−PCR and Western blotting to detect the effect of miR-93-5p on circCDK14 overexpression-mediated promotion of the AFF4 gene. The results showed that the promotion of AFF4 mRNA expression (Fig. 5A) and protein level (Fig. 5B, C) caused by circCDK14 overexpression could be partly abolished by miR-93-5p overexpression. Western blot analysis showed that the increased protein levels of osteogenic markers (OPN and RUNX2) caused by the overexpression of circCDK14 could be relieved by the upregulation of miR-93-5p (Fig. 5D–F). In addition, the elevated ALP (Fig. 5G, H) and ARS (Fig. 5I, J) intensity induced by the upregulation of circCDK14 was reduced by the overexpression of miR-93-5p. Therefore, our findings indicated that circCDK14 could promote the osteogenesis of LF cells via the miR-93-5p/AFF4 pathway.

m6A modification increased circCDK14 expression through the WTAP/IGF2BP3 pathway

To understand why circCDK14 was overexpressed in OLF, we conducted proteomic profiling by MS2-CP-Flag circRNA pull-down assay followed by the mass spectrometry (Fig. 6A). The mass spectrometry showed 228 candidate RBPs were pulled down by the circCDK14. Five important RBPs were obtained by intersecting the proteins from mass spectrometry results and predicted RBPs from RBPsuite (http://www.csbio.sjtu.edu.cn/bioinf/RBPsuite/) (Supplementary Table 4) (Fig. 6B). We paid special attention to WTAP because it is an important RBP relevant to m6A modification [6]. The WTAP was significantly enriched in the pull-down group compared with negative IgG group (Fig. 6C). The RIP assay presented the significant accumulation of circCDK14 transcript by anti-WTAP antibody compared with IgG antibody (Fig. 6D). The qRT-PCR assay (Fig. 6E) and immunohistochemical analysis showed that WTAP was obviously increased in OLF tissues compared to normal LF tissues (Fig. 6F). To explore the effect of WTAP on circCDK14, we transfected the LF cells with siRNAs targeting WTAP. The results showed that the protein level of WTAP (Fig. 6G and H) and RNA level of circCDK14 (Fig. 6I) were obviously reduced when knocking down the WTAP in LF cells. Moreover, the reduction of circCDK14 expression induced by the knockdown of WTAP could be rescued by the overexpression of circCDK14 in LF cells (Fig. 6J). Moreover, we observed that the osteogenic capacity of LF cells could be reduced by the reduction in WTAP, but the suppression could be recused by the overexpression of circCDK14 in the Western blot analysis of osteogenic markers (OPN and RUNX2) (Fig. 6K–M), ALP intensity (Fig. 6N, O), and ARS intensity (Fig. 6P, Q).

Considering the important role of WTAP in the m6A modification, we speculated that WTAP regulated the circCDK14 expression via the m6A modification. Online databases showed that there were several potential m6A modification sites in circCDK14 (Fig. 6R). To further confirm the effects of WTAP on the global m6A level of LF cells, we transfected the siRNAs targeting WTAP to knock down WATP in LF cells. The results showed that reduction of WTAP obviously reduced the m6A level of circCDK14 in LF cells (Fig. 6S), which further decreased the stability of circCDK14 (Fig. 6T). IGF2BP3, another pull-down protein by circCDK14 (Fig. 6B), is a well-known m6A "reading" protein that was reported to bind to m6A modification sites to promote the stability of RNA [6, 20]. Yi et al. reported that IGF2BP3 could recognize and stabilize the circPSMA7 in an m6A-dependent manner [20]. The Western blot showed that IGF2BP3 was significantly enriched in the pull-down group compared with negative IgG group (Fig. 6U). According to our findings, we inferred that the

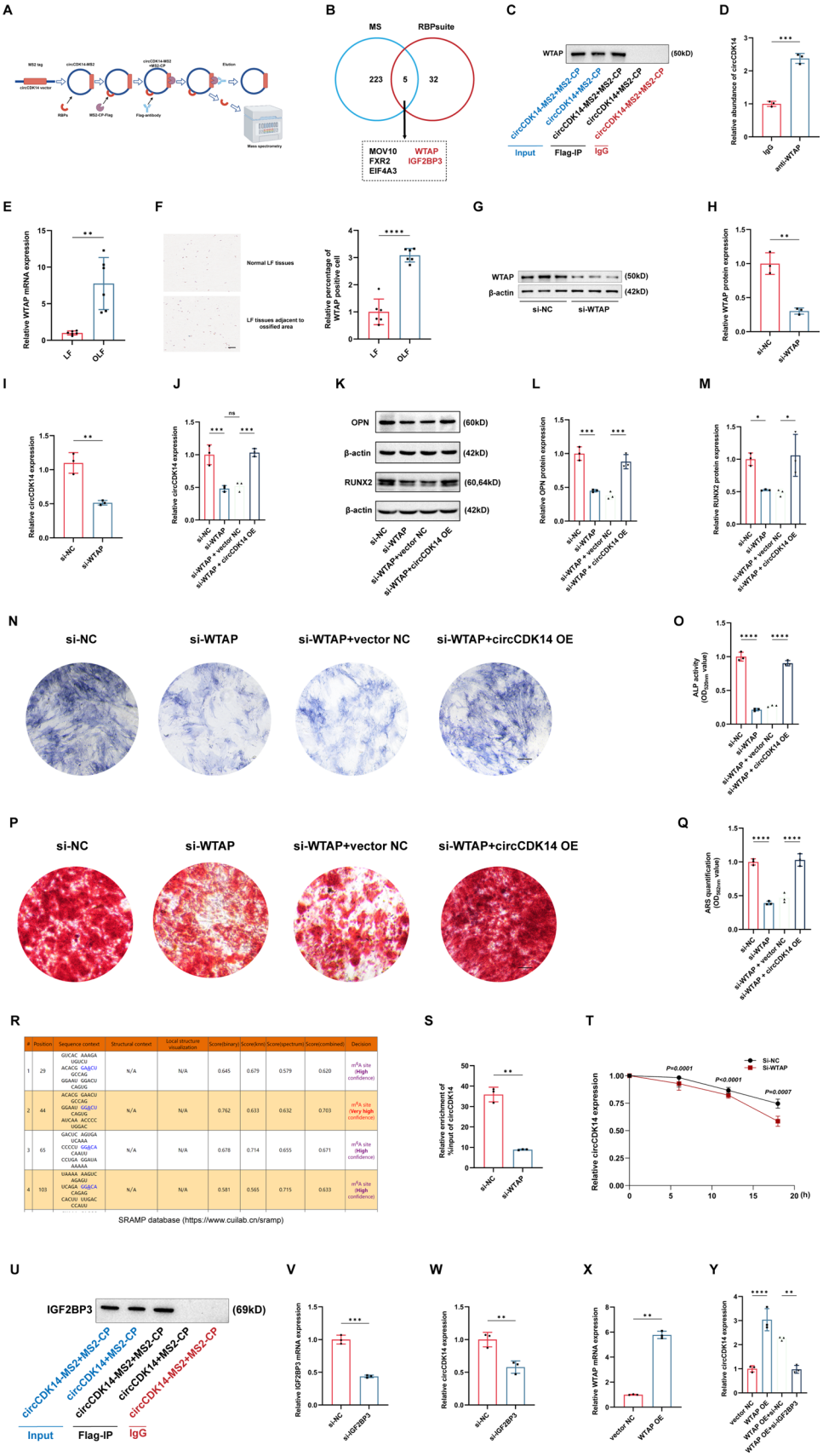

Figure 6 M6A modification increased the circCDK14 expression through the WTAP/IGF2BP3 pathway. **A** CircRNA pull-down using MS2-tagging system, and the following label-free mass spectrometric analysis. **B** Five RBPs of interest after intersecting the pull-down proteins with predicted proteins. **C** Western blot of WTAP pulled down by circCDK14. **D** Significant accumulation of circCDK14 by anti-WTAP antibody. **E**, **F** mRNA (**E**) and protein levels (**F**) of WTAP in LF or OLF tissues (Scale bar = 50 μm). **G**, **H** Protein level of WTAP after the transfection of siRNA targeting WTAP. **I** RNA level of circCDK14 after the knockdown of WTAP. **J** CircCDK14 level after the co-transfection of siRNAs targeting WTAP and circCDK14 overexpression vector. **K**–**M** Protein levels of osteogenic markers (OPN and RUNX2) after the co-transfection of siRNAs targeting WTAP and circCDK14 overexpression vector. **N**–**Q** ALP (**N**, **O**) and ARS (**P**, **Q**) intensity after the co-transfection of siRNAs targeting WTAP and circCDK14 overexpression vector (Scale bar = 25 μm). **R** Predicted m6A sites in circCDK14 by SRAMP database. **S** m6A level of circCDK14 after the WTAP knockdown. **T** Stability of circCDK14 after the WTAP knockdown. **U** Western blot of IGF2BP3 pulled down by circCDK14. **V**, **W** IGF2BP3 (**V**) and circCDK14 (**W**) RNA levels after the IGF2BP3 knockdown. **X** WTAP mRNA level after the transfection of WTAP overexpression vector. **Y** CircCDK14 level after the co-transfection of WTAP overexpression vector and siRNAs targeting IGF2BP3. *MS*, mass spectrometry; *LF*, ligamentum flavum; *OLF*, ossification of the ligamentum flavum; *OE*, overexpression; *ALP*, alkaline phosphatase; *ARS*, Alizarin Red S; * $p < 0.05$, ** $p < 0.01$, *** $p < 0.001$; **** $p < 0.0001$; *ns*, not significant

increased m6A level of circCDK14 caused by WTAP overexpression could be recognized by IGF2BP3, which further promoted the stability of circCDK14. The mRNA level of IGF2BP3 (Fig. 6V) and circCDK14 (Fig. 6W) were both significantly decreased after the transfection of siRNA targeting the IGF2BP3. The mRNA level of WTAP was significantly increased after the transfection of WTAP overexpression vector (Fig. 6X). To validate the effect of the WTAP-IGF2BP3 axis on the stability of circCDK14, we transfected LF cells with a WTAP overexpression vector and siRNAs targeting IGF2BP3, and our results showed that the increase of circCDK14 caused by WTAP overexpression could be relieved by the reduction in IGF2BP3 (Fig. 6Y). These results indicated that circCDK14 expression was upregulated via m6A modification through the WTAP-IGF2BP3 axis during the osteogenesis of LF cells.

In summary, we found that the upregulation of WTAP expression increased the m6A modification in circCDK14, which was further recognized by the IGF2BP3 and promoted the stability of circCDK14. The increased circCDK14 expression further stimulated the osteogenic differentiation of LF cells via the miR-93-5p/AFF4 pathway (Fig. 7).

Discussion

OLF has become the preliminary cause of thoracic spinal stenosis; however, therapeutic options for OLF are limited, and the clinical efficacy is unsatisfactory to date [1, 21]. The main reason for the dilemmas in the treatment of OLF is the complicated and unclear pathogenesis [4]. Therefore, it is urgent to further explore the underlying mechanisms involved in the initiation and progression of OLF with the aim of realizing precise diagnosis and treatment.

CircRNAs, a class of noncoding RNAs generated by pre-mRNA back-splicing, are a crucial compartment of epigenetic modifications [7]. CircRNAs mainly export important biological functions via miRNA sponging, RBPs, and translation into polypeptide chains [7]. CircCDK14 has been proved to play important roles in multiple diseases [9, 11, 17]. For instance, Lai et al. reported that circCDK14 could

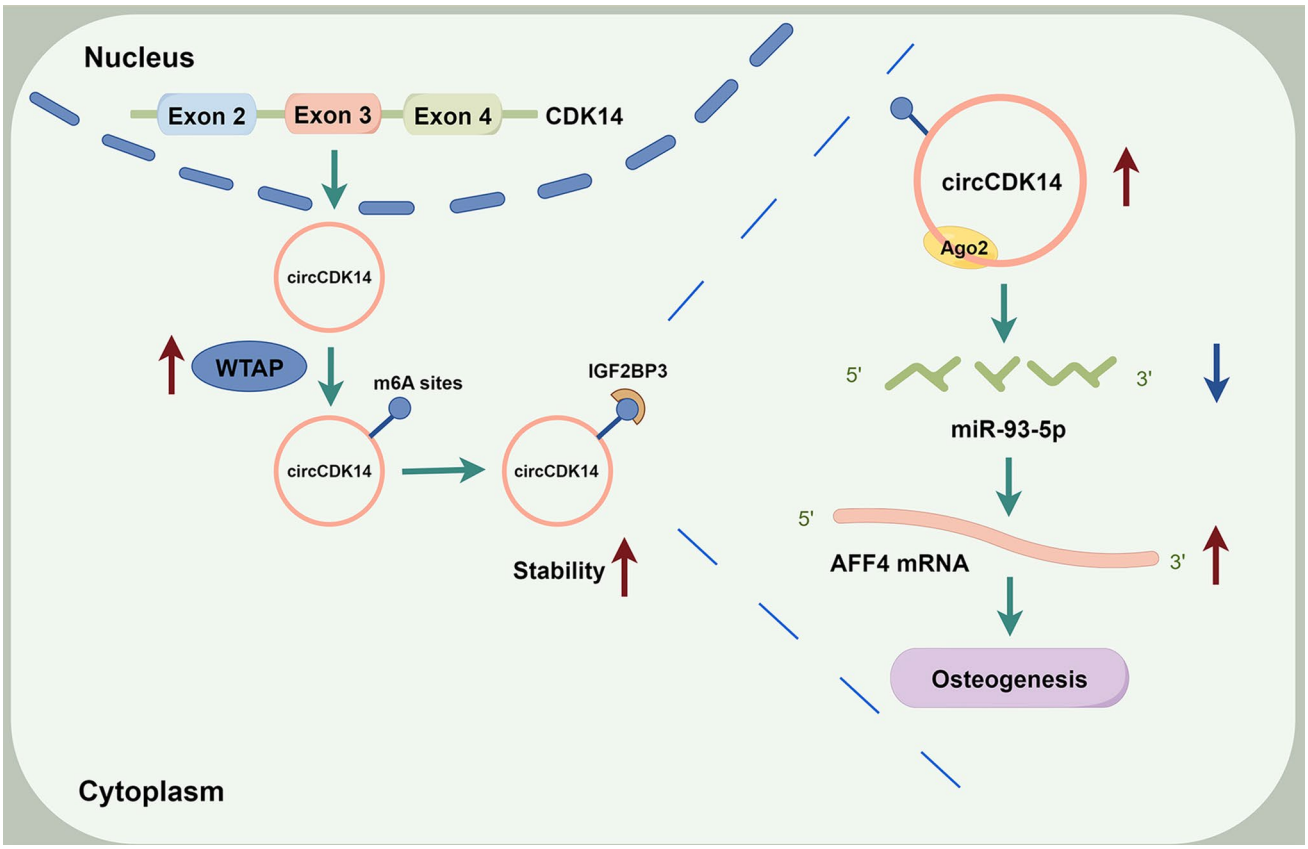

Figure 7 Schematic representation of the investigated mechanisms. The WTAP expression was significantly increased in OLF tissues. The increased WTAP expression elevated the m6A modification level in circCDK14, which was further recognized by the IGF2BP3 and promoted the stability of circCDK14. The increased circCDK14 expression further stimulated the osteogenic differentiation of LF cells via the miR-93-5p/AFF4 pathway

reduce interleukin-1β-induced chondrocyte damage though the miR-1183/KLF5 pathway [17]. Similarly, Shen et al. found that circCDK14 could relieve osteoarthritis through the miR-125a-5p-Smad2 pathway [11]. In neoplastic diseases, Liu et al. found that a reduction in circCDK14 could prevent osteosarcoma progression through the miR-198/E2F2 axis [10]. Chen et al. reported that circCDK14 could regulate PDGFRA, which further promotes tumour progression and resists ferroptosis in glioma [9]. However, no study has been conducted to explore the potential role of circCDK14 in heterotopic ossification diseases, such as OLF.

In this study, circRNA sequencing data showed that circCDK14 is significantly increased in OLF tissues compared to normal LF tissues, which was further confirmed by qRT−PCR. To further investigate the crucial role of circCDK14 in the osteogenic process of LF cells, gain-of-function and loss-of-function assays were conducted, and the results revealed that circCDK14 can obviously promote the osteogenic differentiation of LF cells. Many circRNAs exert their biological functions by sponging microRNAs, which is also named the ceRNA network mechanism [7]. Using the RIP assay, we found that circCDK14 is enriched by AGO2 protein, which indicates that circCDK14 may promote the osteogenic process of LF cells via ceRNA network mechanisms. Bioinformatics analysis predicted that miR-93-5p is a potential target of circCDK14. Several studies reported that the reduction of miR-93-5p could weaken the osteogenic process [22–25], but its role in ectopic ossification has not been reported previously. In this research, we observed that miR-93-5p is downregulated in OLF tissues compared to normal LF tissues, and the overexpression of miR-93-5p reduces the osteogenic capacity of LF cells. More importantly, we identified AFF4 as a potential downstream target of miR-93-5p and found that circCDK14 may increase the expression of AFF4 by sponging miR-93-5p. AFF4, as a core subunit of the superelongation complex, is required for efficient transcription through the release of RNA polymerase II. AFF4 has been proven to be involved in the osteogenic process [18, 26]. Xiao et al. reported that AFF4 promoted the osteogenic differentiation of dental follicle cells by upregulating the transcription of ALKBH1 [18]. Zhou et al. found that a reduction in AFF4 inhibits the osteogenic capacity of marrow mesenchymal stem cells (MSCs) [26]. In Zhu et al. study, the authors reported that AFF4 promoted the osteogenesis of periodontal ligament stem cells though the mTOR-ULK1-autophagy axis [19]. In the current study, for the first time, we found that AFF4 is significantly increased in OLF tissues compared to control LF tissues, which indicates that AFF4 plays key roles not only in normal osteogenic processes but also in ectopic ossification diseases. Furthermore, we demonstrated that AFF4 is upregulated by the circCDK14-miR-93-5p pathway during the osteogenic differentiation of LF cells using rescue assays. To the best of our knowledge, circCDK14 is the first circRNA reported to be associated with the pathogenesis of OLF, and the circCDK14-miR-93-5p-AFF4 pathway was reported to play a crucial role in the progression of OLF.

The m6A modification is the most abundant and well-known RNA modification in eukaryotes [12]. Accumulating evidence indicates that there is a close relationship between m6A modification and the expression level of circRNAs [27]. The m6A modification may affect the expression level of circRNAs by regulating the biogenesis, nuclear export, translation, degradation, and other functions of circRNAs [27]. For instance, Chen et al. reported that circGPATCH2L modified by m6A modification could regulate DNA damage and apoptosis through TRIM28 in intervertebral disc degeneration [28]. Zhong et al. reported that m6A-modified circRBM33 could promote the progression of prostate cancer progression through PDHA1-mediated mitochondrial respiration regulation [29]. Shao et al. found that m6A modification regulated the expression level of circAFF2 via the ALKBH5-YTHDF2 pathway and further enhanced the radiosensitivity of colorectal cancer by inhibiting Cullin neddylation [30]. In a study by Guan et al., the authors announced that m6A-modified circRNA MYO1C was involved in the tumour immune surveillance of pancreatic cancer in a m6A/PD-L1 manner [31]. For OLF, Wang et al. found that ALKBH5 was overexpressed in OLF tissues, which further reduced the RNA methylation level of BMP2 and promoted OLF progression via the AKT signalling pathway [11]. In the m6A modification mechanism, WTAP is a well-known methyltransferase that binds METTL3 and METTL14, forming the methyltransferase complex [32]. WTAP has been reported to promote the osteogenesis of bone MSCs via m6A modification [33]. IGF2BP3 is an important m6A binding protein that generally regulates the stability of RNA by decoding m6A marks [34–37]. Recently, Yi et al. reported that IGF2BP3 could recognize and stabilize the circPSMA7 in an m6A-dependent manner [20]. In this study, for the first time, we discovered that there was a close relationship between WTAP and circCDK14 in the pathogenesis of OLF. WTAP increased the m6A modification level of circCDK14, which was further recognized by IGF2BP3 and enhanced the stability of circCDK14. However, the accurate m6A modification site in circCDK14 recognized by WTAP has not been determined, which needs further investigation. Moreover, it should be noted that animal experiments were not performed in our study, because there is no mature animal model of OLF to date.

In summary, our study shows that increased circCDK14 elevates the expression level of AFF4 by sponging miR-93-5p, which ultimately promotes the osteogenic process of LF cells. In addition, we discovered that m6A modification

increases the stability of circCDK14 via the WTAP-IGF2BP3 pathway. Therefore, circCDK14 may serve as a promising therapeutic target for treating OLF in the future.

Supplementary Information The online version contains supplementary material available at https://doi.org/10.1007/s00018-024-05460-4.

Author contributions LWS designed the research and wrote the manuscript; ZYZ, CLT, and XQ performed the experiments; ZYZ, CLT, and LJL analysed the data; ZYZ, CLT, and JS performed critical reading/editing of the manuscript; LWS supervised the study.

Funding This work was supported by the National Natural Science Foundation of China (Grant No. 82172480).

Data availability The data generated during the current study are available from the corresponding author upon reasonable request.

Declarations

Conflict of interest The authors declare that they have no competing interests.

Ethical approval The experimental protocol was approved by the Ethics Committee of Peking University Third Hospital, and informed consent was obtained from each included patient.

Consent for publication All authors agree with the publication of this article.

References

1. Chen G, Fan T, Yang X, Sun C, Fan D, Chen Z (2020) The prevalence and clinical characteristics of thoracic spinal stenosis: a systematic review. Eur Spine Journal: Official Publication Eur Spine Soc Eur Spinal Deformity Soc Eur Sect Cerv Spine Res Soc 29(9):2164–2172
2. Chen ZQ, Sun CG (2015) Clinical Guideline for treatment of symptomatic thoracic spinal stenosis. Orthop Surg 7(3):208–212
3. Byvaltsev VA, Kalinin AA, Hernandez PA, Shepelev VV, Pestryakov YY, Aliyev MA, Giers MB (2022) Molecular and Genetic Mechanisms of Spinal Stenosis Formation: Systematic Review. Int J Mol Sci 23(21):1
4. Xiang Q, Zhao Y, Lin J, Jiang S, Li W (2022) Epigenetic modifications in spinal ligament aging. Ageing Res Rev 77:101598
5. Li G, Zhang W, Liang H, Yang C (2022) Epigenetic regulation in intervertebral disc degeneration. Trends Mol Med 28(10):803–805
6. Goldberg AD, Allis CD, Bernstein E (2007) Epigenetics: a landscape takes shape. Cell 128(4):635–638
7. Liu CX, Chen LL (2022) Circular RNAs: characterization, cellular roles, and applications. Cell 185(12):2016–2034
8. Xiang Q, Kang L, Wang J, Liao Z, Song Y, Zhao K, Wang K, Yang C, Zhang Y (2020) CircRNA-CIDN mitigated compression loading-induced damage in human nucleus pulposus cells via miR-34a-5p/SIRT1 axis. EBioMedicine 53:102679
9. Chen S, Zhang Z, Zhang B, Huang Q, Liu Y, Qiu Y, Long X, Wu M, Zhang Z (2022) CircCDK14 promotes Tumor Progression and resists ferroptosis in glioma by regulating PDGFRA. Int J Biol Sci 18(2):841–857
10. Liu J, Zhao J, Feng G, Li R, Jiao JJECR (2022) Silencing of circCDK14 suppresses osteosarcoma progression through the miR-198/E2F2 axis. Exp Cell Res 414(1):113082
11. Shen P, Yang Y, Liu G, Chen W, Chen J, Wang Q, Gao H, Fan S, Shen S, Zhao X (2020) CircCDK14 protects against Osteoarthritis by sponging miR-125a-5p and promoting the expression of Smad2. Theranostics 10(20):9113–9131
12. Deng X, Su R, Weng H, Huang H, Li Z, Chen J (2018) RNA N(6)-methyladenosine modification in cancers: current status and perspectives. Cell Res 28(5):507–517
13. Zhu ZM, Huo FC, Pei DS (2020) Function and evolution of RNA N6-methyladenosine modification. Int J Biol Sci 16(11):1929–1940
14. Lin H, Wang Y, Wang P, Long F, Wang T (2022) Mutual regulation between N6-methyladenosine (m6A) modification and circular RNAs in cancer: impacts on therapeutic resistance. Mol Cancer 21(1):148
15. Xu T, He B, Sun H, Xiong M, Nie J, Wang S, Pan Y (2022) Novel insights into the interaction between N6-methyladenosine modification and circular RNA. Mol Therapy Nucleic Acids 27:824–837
16. Lin J, Jiang S, Xiang Q, Zhao Y, Wang L, Fan D, Zhong W, Sun C, Chen Z, Li W (2023) Interleukin-17A Promotes Proliferation and Osteogenic Differentiation of Human Ligamentum Flavum Cells Through Regulation of β-Catenin Signaling. Spine. https://doi.org/10.1097/BRS.0000000000004789
17. Lai X, Song Y, Tian J (2022) CircCDK14 ameliorates interleukin-1β-induced chondrocyte damage by the miR-1183/KLF5 pathway in osteoarthritis. Autoimmunity 55(6):408–417
18. Xiao Q, Zhang Y, Qi X, Chen Y, Sheng R, Xu R, Yuan Q, Zhou C (2020) AFF4 regulates osteogenic differentiation of human dental follicle cells. Int J Oral Sci 12(1):20
19. Zhu L, Wang J, Wu Z, Chen S, He Y, Jiang Y, Luo G, Wu Z, Li Y, Xie J et al (2024) AFF4 regulates osteogenic potential of human periodontal ligament stem cells via mTOR-ULK1-autophagy axis. Cell Prolif 57(2):e13546
20. Yi J, Ma X, Ying Y, Liu Z, Tang Y, Shu X, Sun J, Wu Y, Lu D, Wang X et al (2024) N6-methyladenosine-modified CircPSMA7 enhances bladder cancer malignancy through the miR-128-3p/MAPK1 axis. Cancer Lett 585:216613
21. Zhao Y, Xiang Q, Jiang S, Lin J, Wang L, Sun C, Li W (2023) Incidence and risk factors of dural ossification in patients with thoracic ossification of the ligamentum flavum. J Neurosurg Spine 38(1):131–138
22. Gu Y, Bai Y (2023) LncRNA MALAT1 promotes osteogenic differentiation through the miR-93-5p/SMAD5 axis. *Oral Dis* 30(4):2398
23. Liu C, Zhang Y, Guo J, Sun W, Ji Y, Wang Y, Liu J, Kong X (2023) Overexpression of microRNA-93-5p and microRNA-374a-5p suppresses the osteogenic differentiation and mineralization of human aortic valvular interstitial cells through the BMP2/Smad1/5/RUNX2 signaling pathway. J Cardiovasc Pharmacol 82(2):138–147
24. Zhang Y, Wei QS, Ding WB, Zhang LL, Wang HC, Zhu YJ, He W, Chai YN, Liu YW (2017) Increased microRNA-93-5p inhibits

osteogenic differentiation by targeting bone morphogenetic protein-2. PLoS ONE 12(8):e0182678
25. Zhang Y, Zhuang Z, Wei Q, Li P, Li J, Fan Y, Zhang L, Hong Z, He W, Wang H et al (2021) Inhibition of mir-93-5p promotes osteogenic differentiation in a rabbit model of trauma-induced osteonecrosis of the femoral head. FEBS open bio 11(8):2152–2165
26. Zhou CC, Xiong QC, Zhu XX, Du W, Deng P, Li XB, Jiang YZ, Zou SJ, Wang CY, Yuan Q (2017) AFF1 and AFF4 differentially regulate the osteogenic differentiation of human MSCs. Bone Res 5:17044
27. Han J, Kong H, Wang X, Zhang XA (2022) Novel insights into the interaction between N6-methyladenosine methylation and noncoding RNAs in musculoskeletal disorders. Cell Prolif 55(10):e13294
28. Chen Z, Song J, Xie L, Xu G, Zheng C, Xia X, Lu F, Ma X, Zou F, Jiang J et al (2023) N6-methyladenosine hypomethylation of circGPATCH2L regulates DNA damage and apoptosis through TRIM28 in intervertebral disc degeneration. Cell Death Differ 30(8):1957–1972
29. Zhong C, Long Z, Yang T, Wang S, Zhong W, Hu F, Teoh JY, Lu J, Mao X (2023) M6A-modified circRBM33 promotes prostate cancer progression via PDHA1-mediated mitochondrial respiration regulation and presents a potential target for ARSI therapy. Int J Biol Sci 19(5):1543–1563
30. Shao Y, Liu Z, Song X, Sun R, Zhou Y, Zhang D, Sun H, Huang J, Wu C, Gu W et al (2023) ALKBH5/YTHDF2-mediated m6A modification of circAFF2 enhances radiosensitivity of colorectal cancer by inhibiting Cullin neddylation. Clin Translational Med 13(7):e1318
31. Guan H, Tian K, Luo W, Li M (2023) M(6)A-modified circRNA MYO1C participates in the tumor immune surveillance of pancreatic ductal adenocarcinoma through m(6)A/PD-L1 manner. Cell Death Dis 14(2):120
32. Yang Y, Hsu PJ, Chen YS, Yang YG (2018) Dynamic transcriptomic m(6)a decoration: writers, erasers, readers and functions in RNA metabolism. Cell Res 28(6):616–624
33. You Y, Liu J, Zhang L, Li X, Sun Z, Dai Z, Ma J, Jiao G, Chen Y (2023) WTAP-mediated m(6)a modification modulates bone marrow mesenchymal stem cells differentiation potential and osteoporosis. Cell Death Dis 14(1):33
34. Kuang Y, Li R, Wang J, Xu S, Qiu Q, Lin S, Liu D, Shen C, Liu Y, Xu M et al (2023) ALKBH5-mediated RNA m(6) A methylation regulates the migration, invasion and proliferation of rheumatoid fibroblast-like synoviocytes. Arthritis Rheumatol 1:1
35. Li T, Gu Y, Xu B, Kuca K, Zhang J, Wu W (2023) CircZBTB44 promotes renal carcinoma progression by stabilizing HK3 mRNA structure. Mol Cancer 22(1):77
36. Lin Z, Li J, Zhang J, Feng W, Lu J, Ma X, Ding W, Ouyang S, Lu J, Yue P et al (2023) Metabolic reprogramming driven by IGF2BP3 promotes Acquired Resistance to EGFR inhibitors in Non-small Cell Lung Cancer. Cancer Res 83(13):2187–2207
37. Yang X, Bai Q, Chen W, Liang J, Wang F, Gu W, Liu L, Li Q, Chen Z, Zhou A et al (2023) M(6) A-Dependent modulation via IGF2BP3/MCM5/Notch Axis promotes partial EMT and LUAD Metastasis. Adv Sci (Weinh) 10(20):e2206744